Thesis for the Degree of Master of Engineering

Hydrogel-functionalized Anodic Aluminium Oxide Membranes for Power Generation from Concentration Gradient

by

Iseki Tissasera

Department of Polymer Engineering

The Graduate School

Pukyong National University

February, 2022

Hydrogel-functionalized Anodic Aluminium Oxide Membranes for Power Generation from Concentration Gradient

기능성 하이드로젤이 도입된 양극 산화 알루미늄 멤브레인의 형성과 농도 구배 발전에 대한 연구

Advisor : Prof. Seong Il Yoo

by

Iseki Tissasera

A thesis submitted in partial fulfillment of the requirements
for the degree of

Master of Engineering

in Department of Polymer Engineering, The Graduate School,
Pukyong National University

February, 2022

Hydrogel-functionalized Anodic Aluminium Oxide Membranes for Power Generation from Concentration Gradient

A dissertation

by

Iseki Tissasera

Approved by:

_____

Prof. Joo Hyun Kim

_____ _____

Prof. Kee Seyoung Prof. Seong Il Yoo

February, 25th 2022

CONTENTS

LIST OF TABLES

LIST OF FIGURES

Hydrogel-functionalized Anodic Aluminium Oxide Membranes for Power Generation from Concentration Gradient

Iseki Tissasera

Department of Polymer Engineering,
The Graduate School
Pukyong National University

Abstract

An ion exchange membrane can convert a concentration gradient into electrical energy. Electrochemical gradients flow down ionic currents generated by charged ions moving through membrane channels. Nanopores are able to drive ions substantially better than non-structured membranes, so anodic aluminum oxide (AAO) membrane has previously been utilized as a nanofluidic system. In this study, The surface of AAO membrane was functionalized with 3-(aminopropyl)triethoxysilane (APTES) to enrich the charge density. The APTES-modified AAO was then filled with a positively charged poly(3-acrylamidopropyl) trimethylammonium chloride hydrogel. Then, the energy harvested by these composite membranes was studied by applying them to salted solutions.

기능성 하이드로젤이 도입된 양극 산화 알루미늄 멤브레인의 형성과 농도 구배 발전에 대한 연구

이세키 티사세라

부경대학교 대학원 화학융합공학부

요약

이온 교환막은 농도 구배를 전기 에너지로 변환할 수 있습니다. 전기화학적 구배는 막 채널을 통해 이동하는 하전 이온에 의해 생성된 이온 전류를 따라 흐릅니다. 나노 기공은 구조화되지 않은 멤브레인보다 훨씬 더 나은 이온을 구동할 수 있으므로 양극 산화 알루미늄(AAO) 멤브레인은 이전에 나노 유체 시스템으로 활용되었습니다. 이 연구에서 AAO 멤브레인의 표면은 전하 밀도를 풍부하게 하기 위해 3-(아미노프로필)트리에톡시실란(APTES)으로 기능화되었습니다. APTES로 변형된 AAO를 양전하를 띤 폴리(3-아크릴아미도프로필) 트리메틸암모늄 클로라이드 하이드로겔로 채웠습니다. 그런 다음 이러한 복합 멤브레인에서 수확된 에너지를 염 용액에 적용하여 연구했습니다.

Chapter I. Introduction

I-1. Energy harvesting from concentration gradients

Since fossil fuel sources are limited and global warming is on the rise, renewable energy sources have received significant attention [1]. Electrical energy can be obtained from renewable energy sources through energy harvesting techniques, which have drawn considerable attention as an alternative to meeting energy requirements [2]. Energy harvesting can be utilized from several sources such as motion, thermal, solar/light, radioactive reactions, biological energy, ion-transport-based energy, etc [3-5]. The challenge of accessing low-cost energy from renewable natural resources is key to reducing energy dependence. Recently, concentration gradient energy, which is one of ion-transport-based energy, has received much attention as a nonpolluting, cheap, safe, and sustainable energy source. It is currently under development methods for capturing such osmotic energy, salinity gradient energy, or also known as "blue energy". It has been reported that ion passive transport for salinity gradient energy generation can generate about 5 W/m^2, which has been selected as the target for making salinity gradient power financially viable. However, concentration gradient energy technology has low efficiency. Some research has proposed using pressure-retarded osmosis (PRO) or conventional reverse electrodialysis (RED) to utilize salinity gradient energy, but performance and cost are still limiting a larger-scale application [5-6]. In this way, it is scientifically challenging to improve energy harvesting efficiency from concentration gradient system but is also important to harvest clean energy especially for portable power supplies.

I-2. Ion exchange membrane

In order to capture concentration gradient energy, reverse electrodialysis (RED) is one of the best methods. The method uses selective ion-exchange membranes (IEMs) to transport positive and/or negative ions through water in order to generate power. IEMs are a class of dense polymeric membranes with a fixed charge that carries through their matrix [7-8]. Ion exchange occurs when mobile ions from a liquid phase exchange with ions electrostatically bound to functional groups in a solid. IEMs can be categorized according to the charge and distribution of their fixed ionic group: cation exchange membrane (CEM), anion exchange membrane (AEM), amphoteric IEMs, bipolar membranes, and mosaic IEMs (Figure 1). The CEM and the AEM are monopolar IEMs, and they differ from bipolar membranes CEMs have negatively charged functional groups such as sulfonic acid ($-SO_3-$), carboxylic acid (-COO-), which allow cations to pass but obstruct anions. AEMs have positively charged functional groups such as (ammonium ($-NH_3^+$), secondary amine ($-NRH_2^+$), tertiary amine ($-NR_2H^+$), quaternary amine ($-NR_3^+$), which transport anions but exclude cations [8-12].

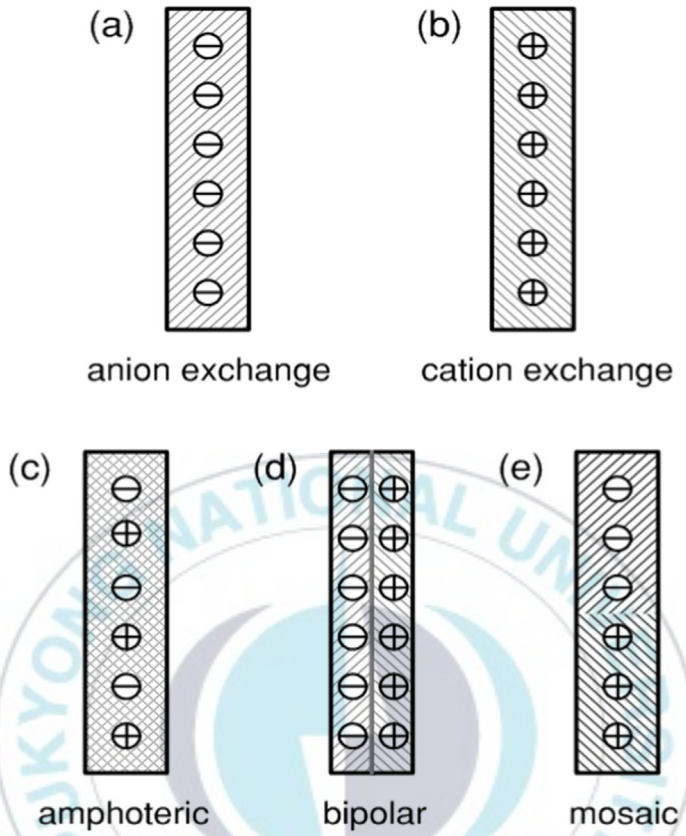

Figure 1. Schematic illustration of the types of IEMs. a) AEMs, (b) CEMs, (c) amphoteric IEMs, (d) bipolar IEMs, and (e) mosaic IEMs. Circles represent the counter-ions in the membrane matrix, while patterns on the background distinguish the different fixed ionic groups [8].

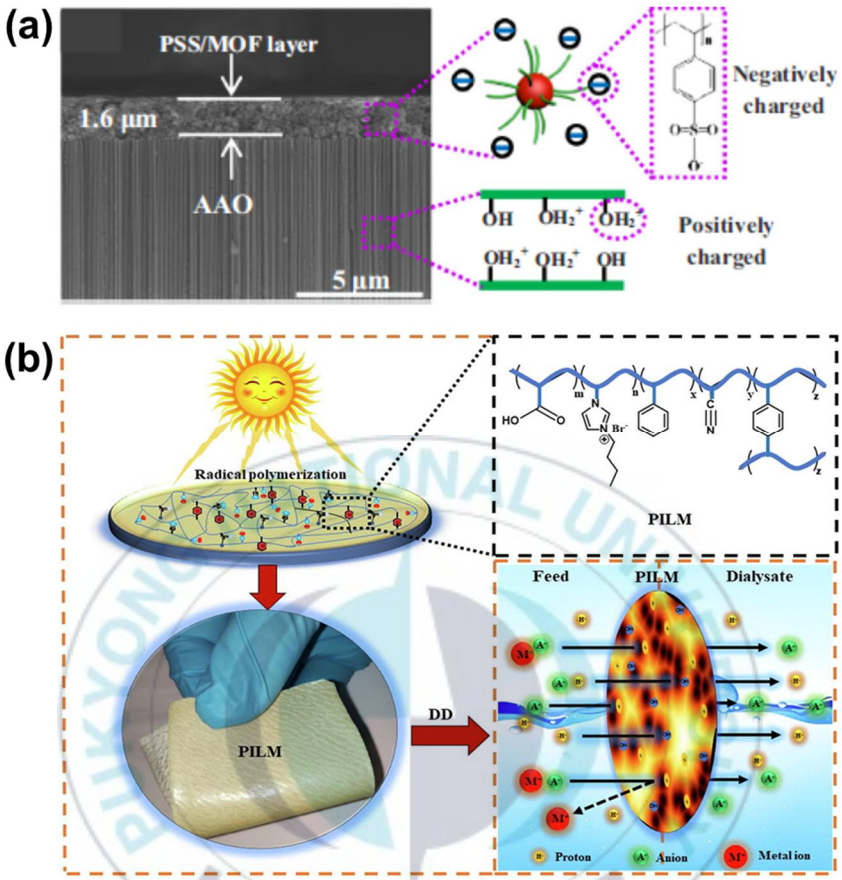

Figure 2. Illustration of the chemical structure of some membranes. (a) PSS/MOF-199 hybrid membrane [13]. (b) Poly (ionic liquid)-based AEMs [14].

As a result of chemical potential in concentration cell, ions are spontaneously translocated from concentrated solution to diluted solution. A chemical potential, as well as known as the Donnan potential, allows the membrane to selectively transmit cations or anions between two solutions [9][15]. Differences between transport numbers of the bulk solution and the membrane result in diffusion at the boundary layers. In the ideal IEM, due to the Donnan exclusion, the electric current is transported by the counter ions. On the other hand, almost all univalent ions carry the same electric current, and therefore excluded ions also polarize in the bulk solution [15]. The Donnan potential has the following expression [8][13] :

$$\varphi_{Don} = \varphi^m - \varphi^s = \frac{RT}{z_i F} ln \frac{a_i^s}{a_i^m} \qquad \text{eq(1)}$$

where φ_{Don} is the Donnan potential, φ^m and φ^s refer to potential of membrane and solution respectively, R belongs to the universal gas constant, T is absolute temperature, F refers to Faraday constant, z_i is valence, a_i^s and a_i^m refer to activity ion i in the solution and membrane respectively [13].

I-2. 1. Ion selectivity

IEMs which have certain physical and electrochemical properties are required to overcome the lack of practical applications of reverse electrodialysis. The membranes should have characteristics such as low electrical resistance, high transport number, and high ion selectivity. Ion selectivity can be illustrated by the ability to separate components from each other on a membrane. [5][8]. A ratio of diffused counterions to diffused counterions can be defined as permselectivity. Permselectivity contributes favorably to understanding membrane potentials: a potential difference (traditionally

called the Nernst potential) naturally arises between two ionic solutions separated by a semipermeable membrane. The permselectivity α, of membrane is given by [15][16] :

$$\alpha = \frac{t_i^m - t_i}{1 - t_i} \quad \text{eq (2)}$$

where t_i^m and t_i refer to counter ion transport number in membrane phase and the bulk solution respectively. Ion transport number of bulk solution is generally constant (i.e. t_+ KCl = 0.490, t_+ NaCl = 0.395), it depends on the mobility ratio of anion and cation. When $t_+ = 1$, the membrane selectively perfectly excludes co ions.

One of the methods to measure evaluate the selectivity of the membrane is Hirtoff method [17]. In this method, two compartments are separated by reversible electrodes similar to Ag/AgCl electrodes. It measures the number of counterions that migrate between the two reservoirs in concentration double cells under constant electric current. The immigrated ions were counted after a certain period, then the unequal potential difference of electrode-salt solution interface generates redox potential (E_{redox}). The measured chemical potential of the membrane cell is open circuit potential (V_{OC}). The value of chemical potentials is different based on the concentration of the solution. The diffusion potential or membrane potential (E_{diff}) is determined by substracting redox potential from measured open circuit potential [17-18] :

$$E_{diff} = V_{OC} - E_{\text{redox}} \quad \text{eq (3)}$$

Then ion transport number of membrane t_i^m can be calculated from the value of diffusion potential. It is given by [20] :

$$E_{diff} = (2t_i^m - 1)\frac{RT}{z_i F} ln \frac{a_i^s}{a_i^m} \quad \text{eq (4)}$$

$$t_i^m = \frac{1}{2}\left(1 + \frac{RT}{z_i F} ln \frac{a_i^s}{a_i^m}\right) \quad \text{eq (5)}$$

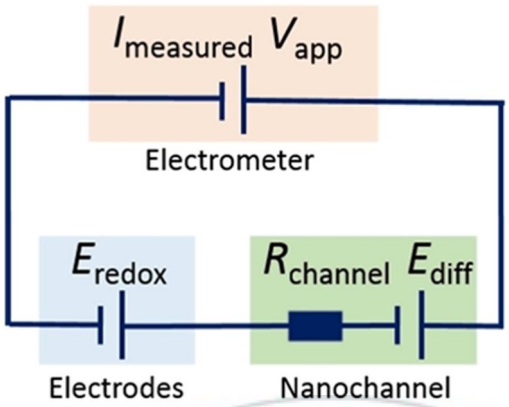

Figure 3. Illustration of the contributions of the different parts of the system to the overall measured current and voltage. $I_{measured}$ is measured electric current and V_{app} is application voltage of electrometer [20].

I-2.2. Nanochannel membranes

A membrane is a selective barrier that allows some substances such as molecules, ions, or other small particles to permeate selectively pass through. Among the membranes, nanochannel membranes are gaining attention nowadays due to their ability to regulate materials in confined spaces, which is particularly relevant to high-resolution sensing and high-efficiency energy conversion [21]. A great deal of research related to energy applications has demonstrated nanochannel membranes made from inorganic materials [22], graphene [23], boron nitride [24], fibers [7], and polymers [2].

Over the past decade, diverse heterogeneous membranes including organic/organic, inorganic/inorganic, and organic/inorganic hybrid system, have been constructed [7][25-27]. The living organisms have developed numerous optimized systems gradients to generate power using such ionic gradients. An electric eel, for example, can utilize highly selective and rectified ion channels to generate significant bio-electricity from fluids containing salts. A hybrid membrane with two or more chemical compositions (heterogeneous membrane) is becoming increasingly popular among researchers. It has the potential for being applied in constructing asymmetric nanochannel membrane systems due to its simplicity. Hybridization of symmetrical/asymmetric homogeneous membranes can easily produce built-in asymmetry. The asymmetric structure, charge, and wettability of the layers would lead to novel ionic transport properties [7][26-28]. Some combination materials to construct heterogeneous asymmetric nanochannel membranes have been reported, such as block copolymer/polyethylene terephthalate [29], modified graphene oxide membrane [30], polyelectrolyte hydrogel/porous aramid nanofiber membrane [7], polymer-

MOF/Anodic alumina hybrid membrane [13], mesoporous silica/alumina membrane [31], graphene/hydrogel membranes [32], and silk nanofibril (SNF)/anodic aluminum oxide membrane [33].

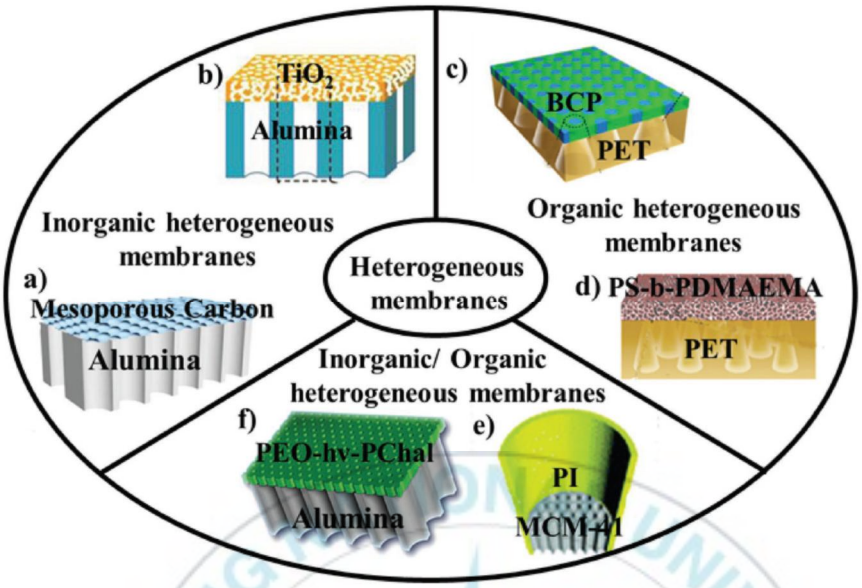

Figure 4. Heterogeneous membranes a) Mesoporous carbon/alumina hybrid membrane [32]; b) TiO_2/alumina heterogeneous nanochannels [34]; c,d) BCP/PET heterogeneous membrane [29]; e) PI/MCM-41 [35]; f) PEO-hv-PChal/alumina composite membrane [36]. [26].

I-3. AAO membranes

Anodic aluminum oxide (AAO), a prime example of the self-ordered electrochemical process, is produced by anodizing aluminum in an acidic electrolyte. It features numerous interesting properties such as high surface area, hardness, chemical stability, and thermal stability. As an inorganic nanochannel, AAO also provides a more robust framework rather than conventional organic membranes. There have been many applications of AAO membranes in recent years, including separation, catalysis, solar cells, fuel cells, bio/chemo sensing, drug delivery, and energy conversion. In all these applications, adequate structural properties of AAO are essential. It can be achieved by modifying the structural and chemical modifications [1][37].

Recent advances in fabrication procedures for structural modification of AAOs with complex pore geometries have been discussed. Those developments result in branched, multilayered, modulated and hierarchically complex pores architectures. Following this, recent progress on surface modification of AAO using wet chemical synthesis and gas phase method has been also presented. This research focuses on tuning the surface of AAO by wet surface modification using silane agent.

I-4. Hydrogel

Hydrogels are crosslinked hydrophilic polymers that do not dissolve in water. The unique and tailorable physiochemical properties of hydrogels have made them an attractive platform for energy and water-related applications. The attractive properties of hydrogels and their derivatives such as ionic and electronic conductivity, electrolyte

permeability, and structural flexibility, can be applied to energy storage systems such as batteries, fuel cells, water-splitting electrolyzers, and concentration gradient power generator. Hydrogel membranes also provide an extensive 3D network of charged ions for efficient interfacial transport. Polymers with anionic (ex : $-NH_3^+$, $-NR_3^+$) or cationic (ex : $-RSO_3^-$, $-RCOO^-$) bonds within their chemical chains form ionic hydrogels. The distribution of ions in an ion-containing hydrogel produces potential energy to drive ion movement in the ion exchange membrane system [7][38-40].

Chapter II. Hydrogel-functionalized Anodic Aluminium Oxide Membranes for Power Generation from Concentration Gradient

II-1. Introduction

Concentration gradient is a type of Gibbs energy that can be extracted into electric energy by using an ion-exchange membrane. As a result of chemical potential, ions move spontaneously from concentrated solution to diluted solution. The unequal distribution of charges on an ion-exchange membrane system caused the Gibbs-Donnan effect. The Gibbs-Donnan effect allows for selective transmission of cations or anions between two solutions. When charges are unequal on electrode surfaces, a redox reaction occurs and this causes electrons to flow along the external circuit. Generally, the flow of electrons through an electrode per unit of time is defined as an electric current. Electricity generated from the harvester then are converted into a useful voltage or current to power the system, or to recharge energy storage devices.

In recent years, functionalized nanochannels have been proposed as a potential alternative to polymer-based ion selective membranes used in energy harvesting devices. Compared to conventional organic membranes, inorganic nanofluidic channels has a more robust framework which caused it may be more suitable for the development of miniaturized power generators and micro-batteries. AAO has several desirable properties as a membrane, such as high surface area, hardness, chemical stability, and thermal stability. Several surface modification strategies are currently being studied to tune the surface properties of AAO. Adding modifications and functionalizing the

surface of AAO will significantly expand the range of applications of AAO-based materials. A wide range of emerging applications will be based on the implementation of this structural engineering and surface manipulation. Surfaces of AAO are chemically unstable in acidic environments, which causes them unsuitable for some applications. A simple way to overcome this issue is to change the surface properties and to add new functionalities to the surface. As AAO surfaces have hydroxyl groups, they can easily be modified by combining them with organic molecules of the desired functionality. There are two main types of surface modification techniques that have been explored to enhance surface properties and introduce new functionality to AAO: wet chemical synthesis techniques and gas-phase techniques. Wet chemical techniques Some of the wet chemical syntheses are self-assembling techniques (silanes, organic acids, and layer-by-layer assembly), polymer grafting, sol-gel processing, electrochemical and electroless deposition [37][41-42]. Silanes can be described as monomeric silicon chemicals. Organosilanes can be described as chemicals that contain at least one carbon-silane bond (Si-C) structure. The molecule can be written as X-R-$Si(OR')_3$. A silane can contain chemically nonreactive or reactive. Nonreactive silanes feature a nonreactive organic group (X : e.g. alkyl), meanwhile reactive silane feature a reactive organic group (X : e.g., amino, vinyl, epoxy, sulfur).

There is a wide range of organofunctional silanes commercially available which have been used as coupling agents or linkers to immobilize polymers and suspended bilayers on AAO surfaces. The Silanization process on AAO surfaces has been proven to be an effective and flexible method to change the wettability and adsorption properties of AAO membranes. [37][41-42]. In this study, the surface properties of AAO was

functionalized by 3-(Aminopropyl)triethoxysilane (APTES). The pKa of bare AAO and APTES is around 6 and 10.0 respectively. When pH = 7, AAO should be positively charged. Due to the presence of amine groups, APTES is expected to enhance positively charged on AAO surfaces [43-45].

Hydrogel membrane provides an extensive 3D network of charged ions for interfacial transport which provides excellent efficiency [7][38]. Hydrogels were prepared using monomers of 3-acrylamidopropyl-trimethylammonium chloride (APTMACl). Poly(APTMACl)is a cationic intelligent material containing a quaternary ammonium salt that presents polymer chains with a natural positive charge. The hydrogel was fabricated by radical polymerization through a crosslinking process [10][38][46]. Herein, we demonstrated hydrogel-functionalized AAO membranes for power generation from concentration gradient. Sequential self-assembly of an organic heterogeneous membrane consisting of one functional membrane layer composed of polyelectrolyte hydrogel and another functionalized AAO membrane was constructed. The inherent electrostatic, asymmetric structure, and stronger charged effect system of the hybrid membranes facilitate anion transport from the functionalized AAO layer to the hydrogel layer.

II-2. Experimental Section

II-2.1. Materials

Aluminium Anodic Oxide (AAO) (13mm/0.02μm) was purchased from iNexus Inc., Korea. 3-(Aminopropyl)triethoxysilane (APTES) (99%), toluene (anhydrous, 99.8%), (3-acrylamidopropyl)trimethylammonium chloride (APTMACl)

(75 wt.%), N,N,N',N'-tetramethylethylenediamine (TEMED), and methyl blue (MB ≈ 60%) were obtained from Sigma-Aldrich. Potassium chloride (KCl) was purchased from Samchum Co,. Korea. Ammonium persulfate (APS) were purchased from Junsei chemical Co,. Japan. N,N'-Methylenebisacrylamide (MBAA) was obtained from Tokyo Chemical Industry Co,. Japan.

II-2.2. Procedure

II-2.2.1. Silane modification of AAO surface

AAO membrane with layered surface functionalities inside the pore channel was prepared by wet chemical techniques with 3-(Aminopropyl)triethoxysilane (APTES). Bare AAO membrane was immersed in 3 wt% of APTES solution diluted in anhydrous toluene for 2 hours. After washing with pure anhydrous toluene, the modified AAO was cured in 120 ^{o}C oven for 1 hour to crosslink the silane layer.

II-2.2.2. Ion exchange capacity and rate of AAO

To determine the ion exchange capacity and rate, the membranes were immersed in an anionic dye, methyl blue (z = -2) aqueous solution. To prepare methyl blue solution, an amount of methyl blue was diluted in water until it reach absorbance ≈ 1. AAO and functionalized AAO were immersed in each 15 mL methyl blue solution and the solution absorbance was measured with a UV-Vis spectroscopy every 30 minutes from 0-120 minutes.

II-2.2.3.Fabrication of APTES-modified AAO/poly(APTMACl)

Poly((3-acrylamidopropyl)trimethylammonium chloride) hydrogel was fabricated by radical polymerization. First, the precursor solution was prepared by dissolving 50 wt% (3-acrylamidopropyl)trimethyl ammonium chloride (APTMACl) and 20 mg MBAA in deionized water. The solution was magnetically stirred at room temperature until homogeneous. Then, the solution was placed in a 40 vacuum oven to remove air bubbles for 30 minutes. After degassing bubbles, 50 μL 20%wt aqueous solution of APS (initiator) and 5 μL TEMED (catalyst) were added into the solution. The precursor solution was poured onto a round-shape mold (2 mm thickness) which was placed onto an APTES-modified AAO membrane. Then, the mold containing precursor solution was covered with a thin glass slide.

II-2.3. Measurement

The membrane morphologies were taken by TESCAN (MIRA 3 LMH in-Beam detector) Field Emission Scanning Electron Microscopy (FE-SEM). The functionalized AAO surface was characterized by X-ray photoelectron spectroscopy (XPS). Electrical measurements were performed with a pair of Ag/AgCl electrode to apply the transmembrane potential in concentration cell. APTES-modified AAO membrane/poly(APTMACl)was mounted between a two-compartment conductivity cell. The effective area of the membrane is ~63.585 mm^2. Using Electrochemical Impedance Spectroscopy (EIS) instruments, ionic conductance was obtained by scanning ionic current and the voltages from -2 V to 2 V for symmetric concentration electrolyte from 1μM to 1M, while energy conversion characteristics of membranes

were studied by scanning ionic current and the voltages from -0.5 V to 0.5 V for concentration gradient of 1 M|10^{-3} M KCl. The maximum power was measured with Keithly 6454 electrometer by obtaining current while applying external resistance to the concentration cell. The power was calculated by equation $P=I^2 \cdot R$.

For applications, the performance of the membrane was conducted by copper electrodes. In terms of maintaining the cleaning of the solution, the rinsing solution ($CuCl_2$) is required in the concentration cell system using copper electrodes. The surfaces of the copper electrode could accumulate impurities without rinse solution. By rinsing, the copper electrode could have a longer lifetime. The 0.1 M $CuCl_2$ solution 3 ml each was added to both the 50 mL concentrated and 50 mL diluted KCl solution in the concentration cell. Furthermore, a series of concentration cells with Cu sheets electrodes (area = ~30 mm x 40 mm) was used to operate small electronic devices (calculator). The concentration-gradient solutions were filled in a series of tiny polycarbonate containers (30 mm x 40 mm x 45 mm). Cells with hydrogel-functionalized AAO membranes were stacked in series to improve electrical performance.

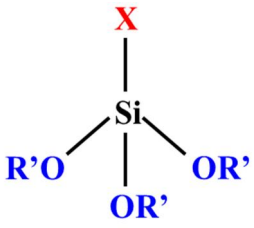

Figure 5. Organosilane structure.

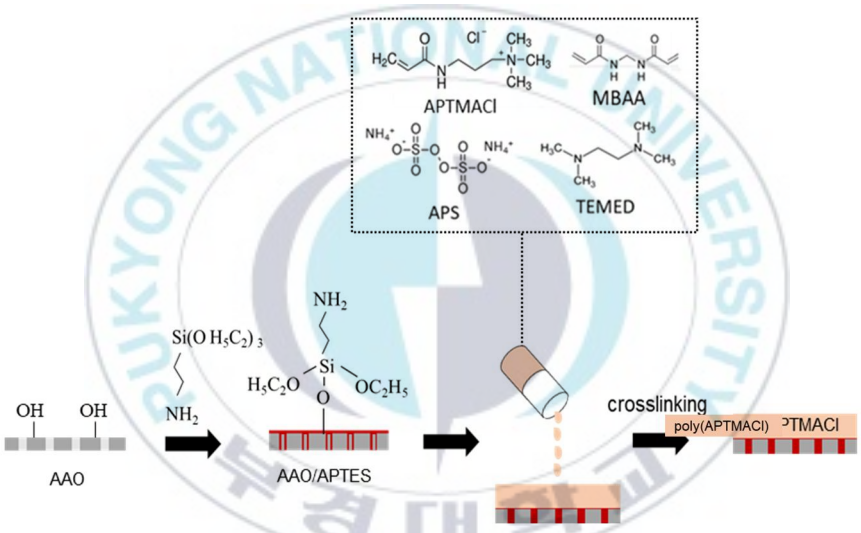

Figure 6. Fabrication of APTES-modified AAO/poly(APTMACl) anion exchange membrane.

II-3. Result and Discussion

II-3.1. Characteristic of AAO and APTES-modified AAO

The AAO surface with the nanochannel arrays of 20 nm in diameter and 60 μm in length was successfully silanized. The Silanization process has been proven to be an effective and flexible method to change the wettability and adsorption properties of AAO membranes [37][41]. As an inorganic nanochannel, AAO also provides a more robust framework rather than conventional organic membranes. In all these applications, adequate structural properties of AAO are essential. It can be achieved by structural and chemical modifications [1][10].

Recent progress on surface modification of AAO has been presented. Modification of AAO surface can be achieved by using wet chemical synthesis and gas phase method. In this work, we focus on tuning the surface of AAO by wet surface modification using a silane agent. Due to the high adhesion of APTES to aluminum oxide, modified AAO appeared roughened compared to the surface of AAO (Figure 7).

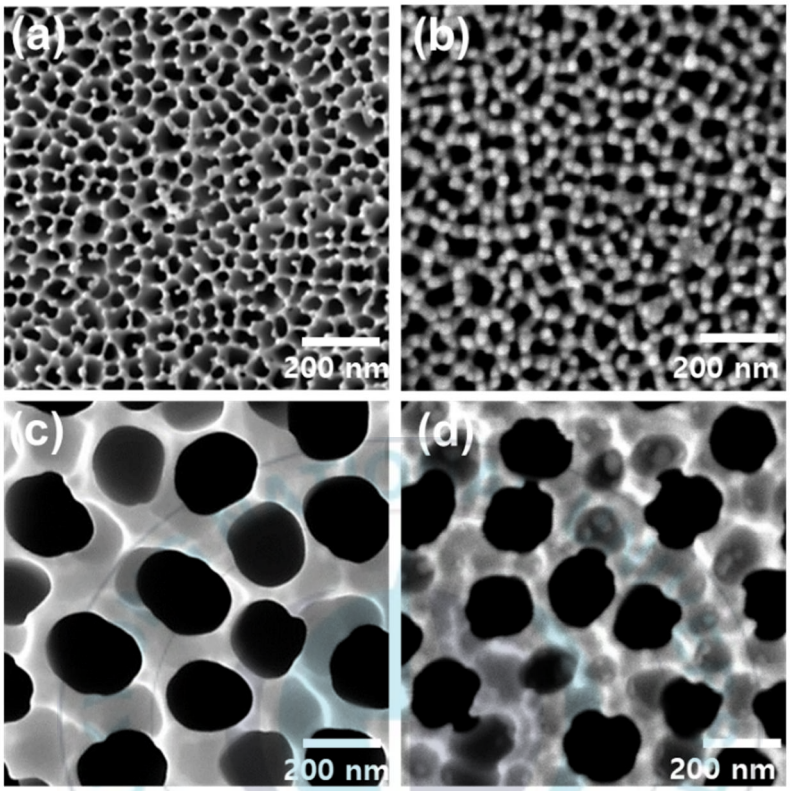

Figure 7. SEM of (a) Top-view and (b) bottom-view of bare AAO. (c) Top-view and (d) bottom-view of APTES-modified AAO.

X-ray photoelectron spectroscopy (XPS) characterization was used to confirm the silane functionalization on AAO channel surfaces. As a result of APTES modification, functionalized AAO was shown to have some XPS spectrums compared to bare AAO. XPS spectra of bare AAO and AAO /APTES were displayed for bands of O1s, Si2p, C1s, N1s, and Al2p. As shown, the peak intensities of O and Al decreased in the oxide layer. It corresponds to the deposit of the hydrolysis products on the AAO surface. Increasing levels of C correlate inseparably with this phenomenon. To be more obvious, N1s and Si 2p XPS spectra are presented. Two peaks were observed in the N1s XPS spectrum NH_2 at 398.8 eV and NH_3^+ at 401.8 eV (Figure 8.d) by APTES-modified AAO, whereas almost no peak of N was spotted around on the surface of bare AAO. (Figure 8.c). In addition, AAO surface after silanization (Figure 8f) shows Si-O-Si (or Si-O-C) band at the peak of 102.1 eV, where previously the surface of bare AAO shows no spectrum of Si (Figure 8e) [18][42][47-48]. These results showed that APTES has been successfully functionalized on the AAO surface.

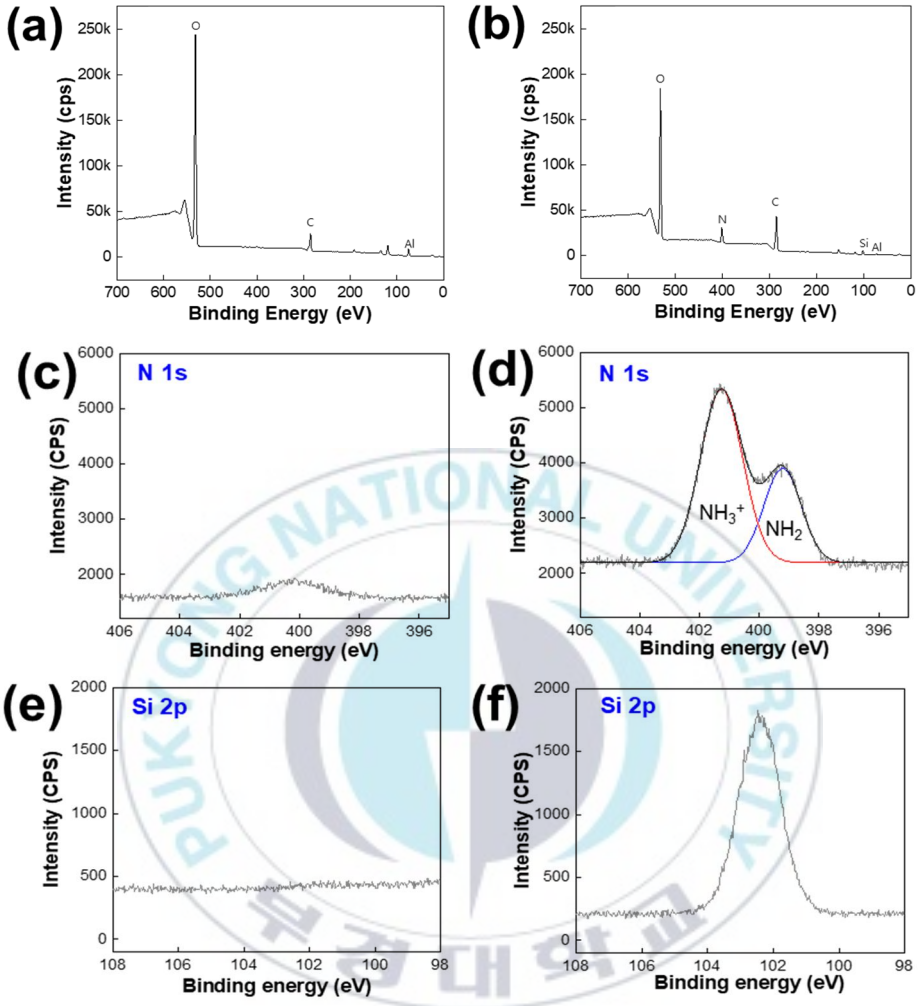

Figure 8. XPS spectrum on bare AAO (a) and APTES-modified AAO (b) surface. XPS spectrum of N1s peak on the surface of (c) bare AAO and (d) APTES-modified AAO. XPS spectrum of Si2p on the surface of (e) bare AAO and (f) APTES-modified AAO.

An anionic dye, methyl blue solution (z = -2), was used to measure dye adsorption. Each membrane was immersed in 20 mL of methyl blue aqueous solution. The maximum methyl blue absorbance was observed every 30 minutes at a wavelength of 585 nm. Using UV-Vis spectroscopy, in Figure 9, it is shown that the absorbance of methyl blue solution at a wavelength of 585 nm decreased by adsorption to the AAO surface. In general, the adsorption rates of APTES-modified AAO (Figure 9b) are faster than bare AAO (Figure 9a). It means that the surface modification of AAO with APTES yields stronger positively charged on AAO surface. It is related to the presence of amine functional groups by APTES, it leads to an enhancement of positively charged surfaces on the AAO channels.

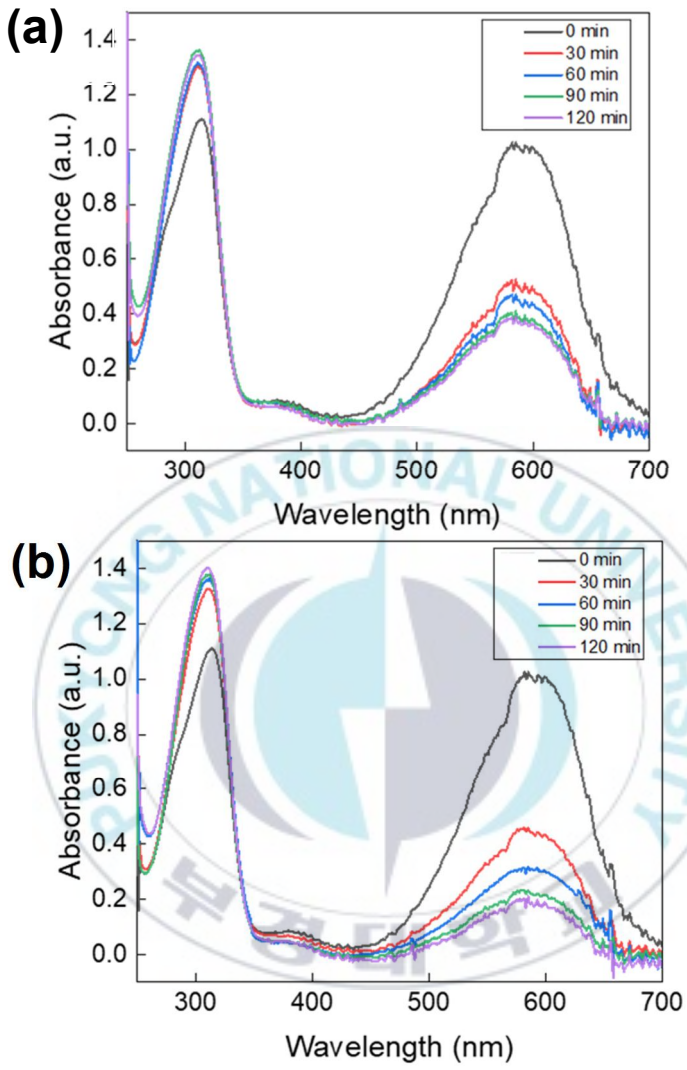

Figure 9. Time-dependent MB absorbance at 583 nm of (a) bare AAO and (b) APTES-modified AAO.

II-3.2. Energy conversion behavior

To measure the energy harvesting performance of the anion-selective membrane, the concentration cell was constructed according to the structure shown in Figure 10. The ionic solution was obtained using 1 M KCl for the concentrated solution (C_H) and a 0.001 M KCl for the diluted solution (C_L). The pH of the KCl solution is around 5.8. Ion exchange membrane systems are driven by concentration gradients or applied electrical fields. Chemical potential causes the ions to migrate spontaneously from concentrated solutions to dilute solutions. Ion exchange membrane systems exhibit the Gibbs-Donnan effect, in which charges are distributed unequally. Since both the gel and the functionalized AAO membranes are positively charged in the ionic solution, the Gibbs-Donnan effect will lead to the movement of only anions (Cl^-) across the hybrid membrane, resulting in diffusion potential and diffusion current. The unequal electrical potential difference between the electrode and salt solution interface generates redox potential. As a result, Ag/AgCl electrodes serve redox reactions that convert ionic current into electric current. From this system, we can measure the open-circuit voltage (V_{OC}) and short-circuit current (I_{SC}) of the membranes.

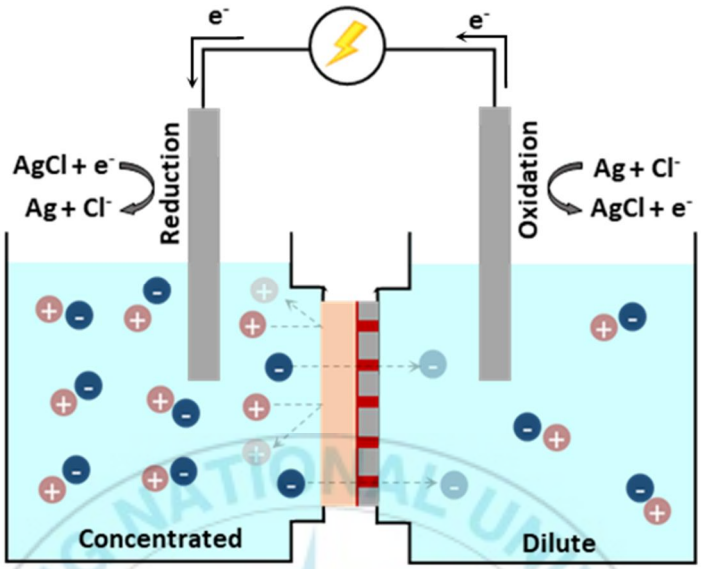

Figure 10. An illustration of a concentration cell.

In order to evaluate the energy conversion behavior of separate and hybrid membranes, we measure the V_{OC} and I_{SC} (Figure 11.b and 11.c). The AAO nanochannels have a positive charge in neutral solution due to their isoelectric point (pI) of about 8–9. In other words, the AAO membrane not only provided a framework for nanochannels but also provided a charge heterojunction in gels [13]. Before silanization, the open-circuit voltage (V_{OC}) and short-circuit current (I_{SC}) of AAO are very low (~6.8 mV to ~0.7 μA). It indicates that bare AAO has very low positively charged. After silanization, V_{OC} and I_{SC} increased to ~11 mV and 1.6 μA, respectively. As the result of surface functionalization by APTES, the presence of amine functional groups leads to an enhancement of positively charged surfaces on the AAO channels. Furthermore, poly(APTMACl) gel with a thickness of 2 mm has higher V_{OC} and I_{SC} rather than functionalized AAO. This can be attributed to its super-hydrophilicity and wider ion transport path. Separately and symmetrically, the AAO and gel membranes act as Ohmic conductors because they are both positively charged and symmetric structures [7]. However, the separate membranes (bare AAO, APTES-modified AAO, and gel) still showed relatively low voltage and current performance compared to hybrid membranes.

The correlation between transmembrane ionic conductance and electrolyte concentration can be seen in Figure 11.c. At 1M , the linear response, a characteristic of charge-neutral channels, agrees well with the bulk conductivity for KCl solution (smooth dashed line) in the given channel geometry. At a low concentration, however, the conductance deviates from a linear regime. When salt concentrations are low, A

higher-than-bulk ionic conductance means that ionic transport in concentration cells is entirely governed by the surface charge of hybrid nanochannel membranes. [13][23].

Noted that in this concentration cell, the electrical potentials (V_{OC}) were accumulated by the diffusion potential of nanochannel membrane (E_{diff}), the potential between two Ag/AgCl electrodes ($E_{electrode}$), and concentration gradient redox potential (E_{redox}). E_{diff} is created when ions are selectively moved along the membrane. In the case of identical electrodes, the $E_{electrode}$ becomes zero. Meanwhile, E_{redox} potential results from the unequal drop in potential at the electrode-solution interface. Using the equivalent circuit of the power generating system, E_{diff} can be obtained by subtracting the difference in redox potential the measured electrical potential (V_{OC}), as shown as an equation :

$$E_{diff} = V_{OC} - E_{\text{redox}} \qquad \text{eq (3)}$$

Ion transport number (t) can be calculated using the equation :

$$t_i^m = \frac{1}{2}\left(21 + \frac{RT}{z_i F} ln \frac{a_i^s}{a_i^m}\right) \qquad \text{eq (5)}$$

The concentration gradient redox potential was obtained by measuring the potential of separated salt solution reservoirs connected to a saturated KCl salt bridge. Concentration gradients have different redox potentials. The redox potential of 1 M | 0.001 M KCl is 11.4 mV. The calculated membrane diffusion potential and ion transport number of nanochannel membranes are shown in Table 1. Ion transport of bare AAO is 0.49. In other words, the co-ion and counter-ion passed through the membrane almost at a similar rate. As t approaches 1, ion selectivity increases, which indicates hybrid membranes are better able to select anion.

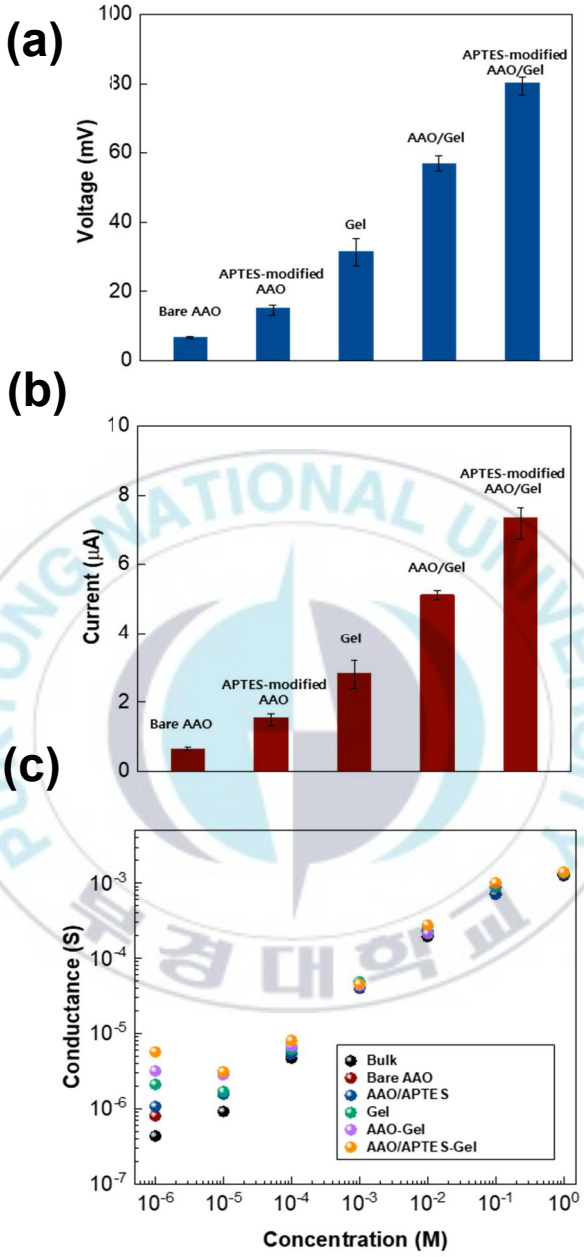

Figure 11. (a) Open-circuit voltage and (b) Short-circuit current of concentration cells of membranes. (c) The transmembrane ionic conductance.

Membranes	VOC (mV)	Ediff (mV)	Ion transport number
AAO	6.84	-4.54	0.49
APTES-modified AAO	11.01	-0.36	0.51
Gel	31.55	20.17	0.56
AAO/Gel	56.8	45.42	0.64
APTES-modified AAO/Gel	80.28	68.90	0.71

Table 1. The summarizes of $V_{OC,}$ $E_{diff,}$ and ion transport number of membranes

II-3.3. Enhanced energy harvesting performance

The I-V curve of hybrid membranes was recorded to further examine the energy conversion properties. Intercepts on the voltage axis equal the transmembrane diffusion potential, which equals the open-circuit voltage, whereas intercepts on the current axis equals the short circuit current. The concentration gradients can be arranged according to two different configurations (Figure 12.a). In the case of high concentration solution placed on the gel side (forward direction), the V_{oc} and I_{sc} are 80.2 mV and 7.4 μA, respectively. In the presence of a reverse concentration gradient with a high concentration on the functionalized AAO side, the V_{oc} and I_{sc} decrease to ~56.7 mV and ~5 μA, respectively (Figure 12b). Based on this observation, the asymmetric membrane systems, the different local concentrations of membrane charged, and the fluid transport, are still responsible for causing a preferential direction of ion transport under salinity gradients. The synergistic effect of the two functional layers can explain such a directional and high energy performance output. As the APTES-modified AAO side and hydrogel side has different charged local concentration, the ion is transported from the APTES-modified AAO side to the hydrogel side (or revised direction), which means that charge polarization affects the efficiency of ion-selective nanopores [49].

Channel length influences the ion selectivity of nanochannels as well, which is vital for osmotic energy conversion. Further investigation of the influence of membrane thickness on V_{oc} and I_{sc} was performed with a concentration gradient of 1M|0.001M KCl. The thickness of the gel plays a significant role in determining how

much energy is generated. The 3D charged network of gel membrane will contribute substantially to the increased interfacial transport. The thickness of the hybrid membrane can be controlled by the difference in the thickness of the mold used to accommodate the hydrogel precursor on the APTES-modified AAO membrane. In Figures, 12c and 12d, an increase of V_{oc} and I_{sc} were observed upon decreasing the channel length. Reducing the length of the nanochannel has the effect of reducing the resistance of the membranes. As current density increases, so does the number of counterion transporters; however, this increase is more pronounced for membranes with smaller fixed charge density values. However, when the gel layer is too thin, the functional groups become insufficient to function optimally. Further investigation will be required to develop a comprehensive understanding.

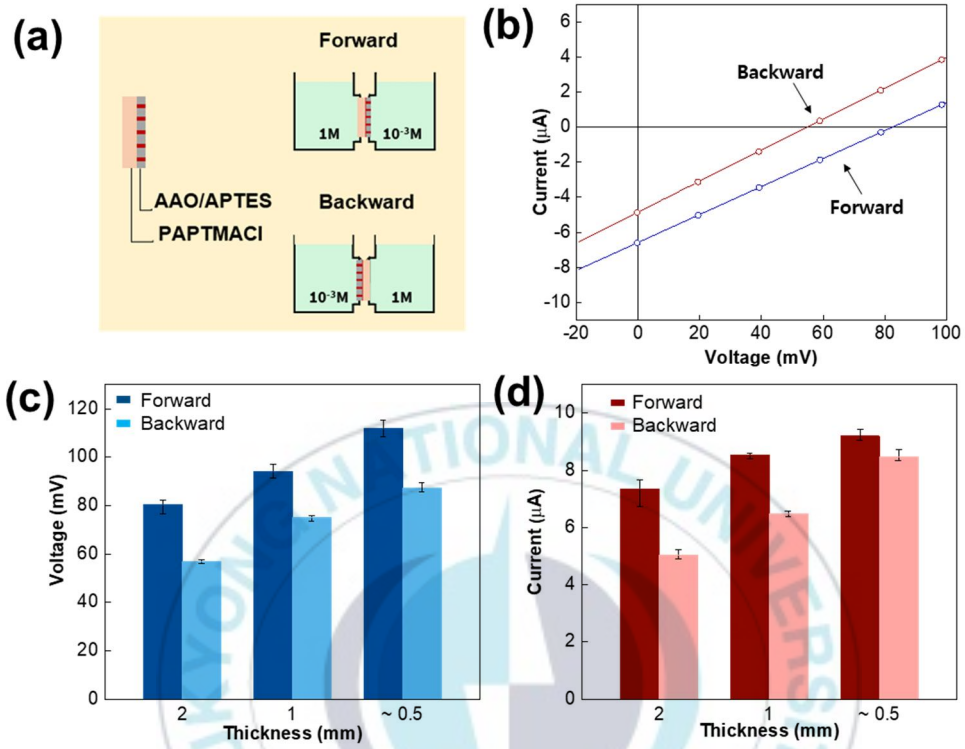

Figure 12. (a) Configurations of the directions of concentration-gradient cells. (b) I-V curves of APTES-modified AAO/poly(APTMACl)under forward and backward direction. (c)Open-circuit voltage and (d) Short-circuit current upon decreasing the thickness of the membrane. Concentration gradient of 1M|0.001M KCl.

Furthermore, we investigated the dependence of V_{oc} and I_{sc} on the concentration gradients. As the basic concentration gradient used in the previous observations was 1M|0.001M, we test both for higher and lower concentration gradients. The KCl concentration on the concentrated side was kept at 1M and the diluted side was varied (0.1 M, 0.01M, 0.001M, and 0.0001M KCl. The concentration gradient drives ion diffusion, so a higher concentration gradient was assumed to result in a higher concentration. In Figure 13a, for concentration gradient from 10 to 1000, V_{oc} seems to increase but decreases with a further increase in $C_H|C_L$. It may be caused by the diameter of nanochannels, the small (~20 nm) led to a strong overlapping of the effect of an electrical double layer (EDL) when the concentration gradient was too high [50]. From diffusion potential, we can calculate the transference number of anions (Cl^-), by equation 4.

$$E_{diff} = (2t_i^m - 1)\frac{RT}{z_i F} ln \frac{a_i^s}{a_i^m} \qquad \text{eq (4)}$$

Increasing KCl concentration reduced the thickness of the EDL, resulting in a smaller value of Cl^- transference number and less anion-selectivity. A concentration gradient of 1000 produced the maximum V_{oc} of ~112 mV. Figure 13b shows the variation of I_{sc} with different $C_H|C_L$. As shown, the magnitude of I_{sc} increases from 10 to 100-folds, But when $C_H|C_L$ was 1000, it decreases. This may be due to the weaker effect of surface charge at high concentration gradients [51-52]. A concentration gradient of 100 produced the maximum I_{sc} for about 44 μA.

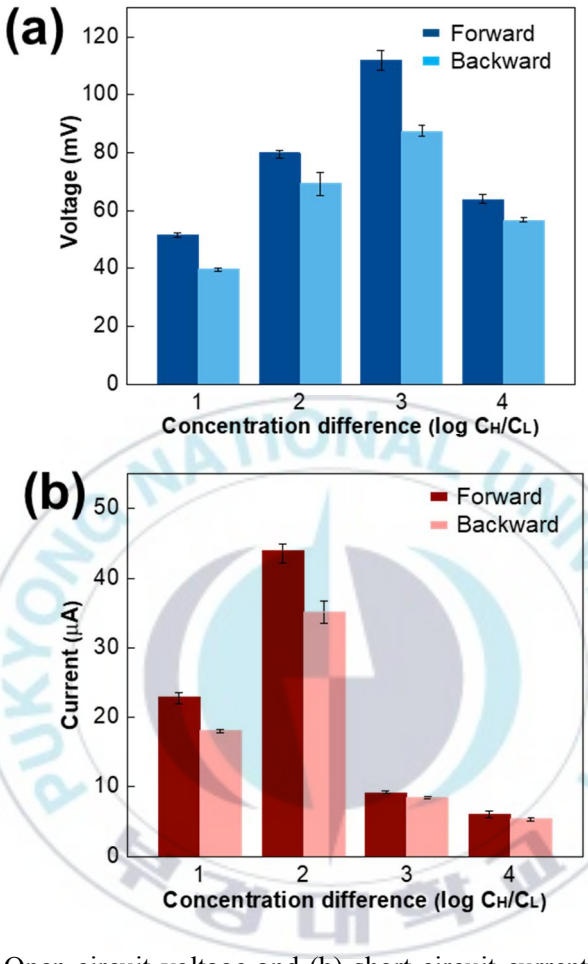

Figure 13. (a) Open-circuit voltage and (b) short-circuit current of APTES-modified AAO/poly(APTMACl) in the different concentration gradients. C_H is fixed at 1M.

II-3.4. Applications

Hydrogel-functionalized AAO membranes with a thickness of ~500 μm applied in the forward direction of the concentration gradient of 1M | 0.001M KCl showed the best result. In the next step, we connected an external resistance the concentration cell to measure the power. Anode and cathode of the Ag/AgCl reference electrodes have the same reaction which gives zeroes net potential. In this case, besides using Ag/AgCl electrodes, we also utilized copper electrodes. Figure 14.a shows the comparison of V_{oc} and I_{sc} between Ag/AgCl and copper electrodes. V_{OC} of concentration cells using Ag/AgCl and copper electrodes are electrodes ~75 mV and ~149 mV respectively. Meanwhile, the I_{sc} is ~44 μA and ~48 μA respectively. Next, Figure 14.b shows the output power generated by concentration cells. With the Ag/AgCl electrodes system, the cell generated 0.41 μW of P_{max}, whereas using copper electrodes system, the power significantly increases to 1.43 μW.

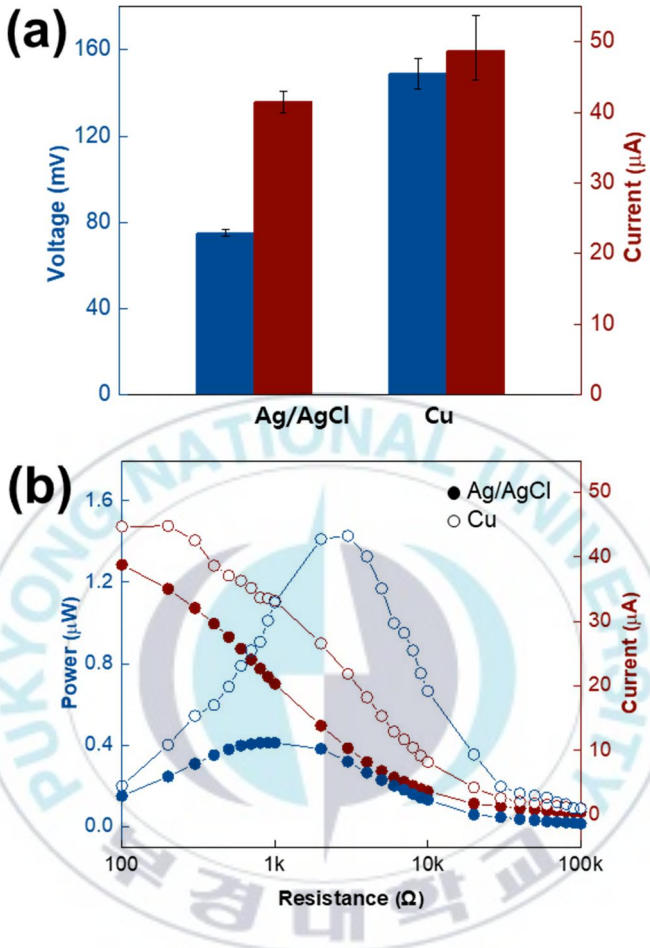

Figure 14. (a) Open circuit voltage and short circuit current; (b) Output current and power under external load resistance using different electrodes. Concentration difference of KCl 1M|0.01M.

Furthermore, a series of concentration cells with Cu sheets electrodes was also used to enhance power. The concentration-gradient solutions were filled in a series of tiny polycarbonate containers. Cells with hydrogel-functionalized AAO membranes were stacked in series to improve electrical performance. Figure 15a shows that the output voltage increased linearly with the number of stacked cells, whereas almost no changes have been observed in the output current. A stack of 10 cells yielded a V_{OC} of 1.47 V or produced an average value of 147 mV per cell. These average values are comparable with the V_{OC} in Figure 15a (149 mV). This series reached 14 μW of output power from the external resistance, which corresponded to an average value of 1.47 μW per cell. It is also comparable with Figure 15. b (1.4 μW). It means that the energy harvesting performance of the system is linearly proportional to the number of stacked cells used in the system. Ten series of stacked hydrogel-functionalized AAO (Figure 15.c) can be applied to operate small devices such as a calculator (Figure 15.d).

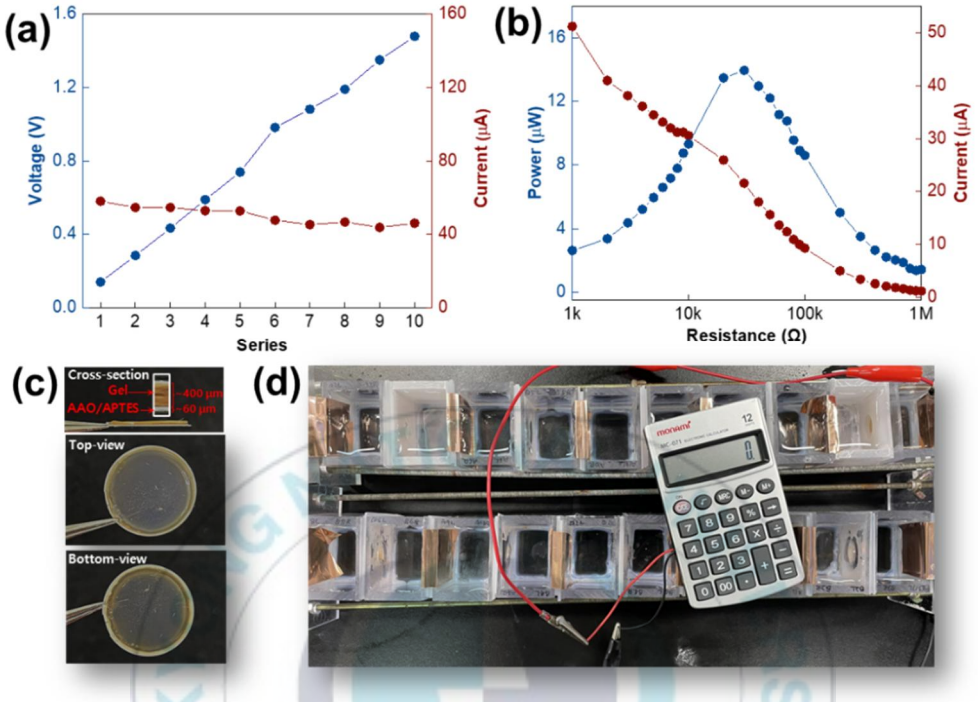

Figure 15. (a) Open circuit voltage and short circuit current of stacked concentration cells in series. (b) Output current and power generated by 10 series concentration cells under external load resistance. (c) APTES-modified AAO/poly(APTMACl) membrane. (d) Operating a calculator with 10 series concentration-gradient cells. Concentration difference of KCl 1M|0.01M.

II-4. Conclusion

In summary, we have constructed an asymmetry hybrid nanochannel exchange membrane by synthesizing charged polyelectrolyte hydrogel onto a functionalized AAO membrane for concentration-gradient cell application. The presence of amine functional groups from APTES functionalization enhances the positively charged surfaces of AAO channels. Meanwhile, poly-APTMACl hydrogels accelerate ion diffusion and interfacial transport efficiency through a wide 3D network charged. The asymmetric structure, higher charge, and inherent electrostatic properties of hybrid membranes provide great local ionic effect systems, facilitating the transport of anions from the functionalized AAO layer to the hydrogel layer. A concentration cell can produce V_{OC} up to ~149 mV and Isc ~48 μA. Despite the limited amount of electric energy harvested from a single cell, this value still has great potential for practical applications. The combination of concentration-gradient cells of hybrid membranes significantly increased the output power to supply small electronic devices. This work could be a basic example to stimulate further experimental and theoretical studies of AAO membranes and polyelectrolyte gels for wider application.

References

[1] Kim, J., Kim, S.J. and Kim, D.K., (2013), *Energy*, **51**, 413-421.

[2] Koo, J.M., Park, C.H., Yoo, S., Lee, G.W., Yang, S.Y., Kim, J.H. and Yoo, S.I., (2021), *Soft Matter*, **17,** 13, 3700-3708.

[3] Harb, A., (2011), *Renewable Energy*, **36**, 10, 2641-2654.

[4] Muhthassim, B., Thian, X.K. and Hasan, K.M., (2018), In *IOP Conference Series: Earth and Environmental Science* , **140**, 1, p. 012045).

[5] Hong, J.G. and Chen, Y., (2014), *Journal of Membrane Science*, **460**, 139-147.

[6] Balme, S., Ma, T., Balanzat, E. and Janot, J.M., (2017), *Journal of Membrane Science*, **544**, 18-24.

[7] Zhang, Z., He, L., Zhu, C., Qian, Y., Wen, L. and Jiang, L., (2020), *Nature communications*, **11**, 1, 1-8.

[8] Luo, T., Abdu, S. and Wessling, M., (2018), *Journal of membrane science*, **555**, 429-454.

[9] Cobzaru, C., & Inglezakis, V. (2015), *Progress in Filtration and Separation*, 425–498.

[10] Hong, J.G., Gao, H., Gan, L., Tong, X., Xiao, C., Liu, S., Zhang, B. and Chen, Y., (2019), *Advanced Nanomaterials for Membrane Synthesis and its Applications* (295-316).

[11] Emmanuel, K., Cheng, C., Erigene, B., Mondal, A.N., Hossain, M.M., Khan, M.I., Afsar, N.U., Liang, G., Wu, L. and Xu, T., (2016), *Journal of Membrane Science*, **497**, 209-215.

[12] Fan, H. and Yip, N.Y., (2019), *Journal of Membrane Science*, **573**, 668-681.

[13] Li, R., Jiang, J., Liu, Q., Xie, Z. and Zhai, J., (2018), *Nano Energy*, **53**, 643-649.

[14] Naik, N.S., Padaki, M., Déon, S. and Murthy, D.H., (2020), *Chemical Engineering Journal*, **401**, p.126148.

[15] Zhao, W., Gong, H., Song, Y., Li, B., Xu, N., Min, X., Liu, G., Zhu, B., Zhou, L., Zhang, X.X. and Zhu, J., (2021), *Advanced Functional Materials*,

p.2100025.

[16] Avci, A.H., Tufa, R.A., Fontananova, E., Di Profio, G. and Curcio, E., (2018), *Energy*, **165**, 512-521.

[17] Geise, G.M., Cassady, H.J., Paul, D.R., Logan, B.E. and Hickner, M.A., (2014), *Physical Chemistry Chemical Physics*, **16**, 39, 21673-21681.

[18] Wojciechowski, J., Szubert, K., Peipmann, R., Fritz, M., Schmidt, U., Bund, A. and Lota, G., (2016), *Electrochimica Acta*, **220**, 1-10.

[19] Strathmann, H., Grabowski, A. and Eigenberger, G., (2013), *Industrial & Engineering Chemistry Research*, **52**, 31, 10364-10379.

[20] Huang, X., Zhang, Z., Kong, X.Y., Sun, Y., Zhu, C., Liu, P., Pang, J., Jiang, L. and Wen, L., (2019), *Nano Energy*, **59**, 354-362.

[21] Zhu, Y., Zhan, K. and Hou, X., (2018), *Acs Nano*, **12,** 2, 908-911

[22] Kim, J., Kim, S.J. and Kim, D.K., (2013), *Energy*, **51,** 413-421.

[23] Hong, S., Ming, F., Shi, Y., Li, R., Kim, I.S., Tang, C.Y., Alshareef, H.N. and Wang, P., (2019), *ACS nano*, **13**, 8, 8917-8925.

[24] Qin, S., Liu, D., Wang, G., Portehault, D., Garvey, C.J., Gogotsi, Y., Lei, W. and Chen, Y., (2017), *Journal of the American Chemical Society*, **139***,* 8, 6314-6320.

[25] Zhu, X., Hao, J., Bao, B., Zhou, Y., Zhang, H., Pang, J., Jiang, Z. and Jiang, L., (2018), *Science advances*, **4**, 10, p.eaau1665.

[26] Li, R., Fan, X., Liu, Z. and Zhai, J., (2017), *Advanced Materials*, **29**, 45, p.1702983.

[27] Zhang, Z., Wen, L. and Jiang, L., (2018), *Chemical Society Reviews*, **47**, 2, 322-356.

[28] Chakrabarty, T., Rajesh, A.M., Jasti, A., Thakur, A.K., Singh, A.K., Prakash, S., Kulshrestha, V. and Shahi, V.K., (2011), *Desalination***, 282**, 2-8.

[29] Zhang, Z., Kong, X.Y., Xiao, K., Liu, Q., Xie, G., Li, P., Ma, J., Tian, Y., Wen, L. and Jiang, L., (2015), *Journal of the American Chemical Society*, **137**, 46, 14765-14772.

[30] Wang, L., Feng, Y., Zhou, Y., Jia, M., Wang, G., Guo, W. and Jiang, L.,

(2017), *Chemical science*, **8,** 6, 4381-4386.

[31] Gao, J., Guo, W., Feng, D., Wang, H., Zhao, D. and Jiang, L., (2014), *Journal of the American Chemical Society*, **136***,* 35, 12265-12272.

[32] Zhan F, Wang Z, Wu T, Dong Q, Zhao C, Wang G, Qiu J. (2018), *Journal of Materials Chemistry A*, **6,** 12:4981-7.

[33] Xin, W., Zhang, Z., Huang, X., Hu, Y., Zhou, T., Zhu, C., Kong, X.Y., Jiang, L. and Wen, L., (2019), *Nature communications*, **10***,* 1, 1-10.

[34] Q. Q. Zhang, Z. Y. Hu, Z. Y. Liu, J. Zhai, L. Jiang, (2014), *Adv. Funct. Mater,* **24**, 424.

[35] Zhang, W., Meng, Z., Zhai, J. and Heng, L., (2014), *Chemical Communications*, *50*(27), 3552-3555.

[36] Sui, X., Zhang, Z., Zhang, Z., Wang, Z., Li, C., Yuan, H., Gao, L., Wen, L., Fan, X., Yang, L. and Zhang, X., (2016), *Angewandte Chemie International Edition*, **55***,* 42, 13056-13060.

[37] Jani, A.M.M., Losic, D. and Voelcker, N.H., (2013), *Progress in Materials Science*, **58**, 5, 636-704.

[38] Guo, Y., Bae, J., Fang, Z., Li, P., Zhao, F. and Yu, G., (2020), *Chemical reviews*, **120***,* 15, 7642-7707.

[39] SM, Mark, C. A. Finch, Martin T.. Goosey, and B. N. Hendy, (1987), *Specialty polymers*

[40] Zhao, F., Shi, Y., Pan, L. and Yu, G.,(2017), *Accounts of chemical research*, **50** ,7, 1734-1743.

[41] Jani, A.M.M., Yazid, H., Habiballah, A.S., Mahmud, A.H. and Losic, D.,(2015), *Nanoporous Alumina* (155-184). Springer, Cham.

[42] Kwak, S.H., Kwon, S.R., Baek, S., Lim, S.M., Joo, Y.C. and Chung, T.D., (2016), *Scientific reports*, **6,** 1, 1-8.

[43] Seehuber, A., Schmidt, D. and Dahint, R., (2012), *Langmuir*, 28, 23, 8700-8710.

[44] Materne, T., de Buyl, F. and Witucki, G.L., (2012), *Dow Corning Corporation*, 1-16.

[45] Cho, Y., Lee, C. and Hong, J., (2014), *Colloids and Surfaces A: Physicochemical and Engineering Aspects*, **443**, 195-200.

[46] Mohammadi, Z., Ghorbanloo, M. and Mokari, T., (2020), *Nanochemistry Research*, **5**, 2, 211-224.

[47] Alrayyes, A.U., Hu, Y., Tabor, R.F., Wang, H. and Saito, K., (2021), *Journal of Materials Chemistry A*, **9**, 37, 21167-21174.

[48] Dhahri, S., Fazio, E., Ghrib, M., Neri, F., El Khirouni, K. and Ezzaouia, H., (2017), *Journal of Alloys and Compounds*, **699**, 991-997.

[49] Siria, A., Bocquet, M.L. and Bocquet, L., (2017), *Nature Reviews Chemistry*, **1**, 11, 1-10.

[50] Yan, F., Yao, L., Chen, K., Yang, Q. and Su, B., (2019), *Journal of Materials Chemistry A*, **7**, 5, 2385-2391.

[51] Guo, W., Cao, L., Xia, J., Nie, F.Q., Ma, W., Xue, J., Song, Y., Zhu, D., Wang, Y. and Jiang, L., (2010), *Advanced functional materials*, **20**, 8, 1339-1344.

[52] Yang, Q., Lin, X., Wang, Y. and Su, B., (2017), **9**, 46, 18523-18528.

Acknowledgements

I would like to express my gratitude to my advisor, Professor Seong Il Yoo, for his guidance and support. While researching, professor directing helped me to understand the experiments. It was an opportunity to learn a wider and deeper knowledge as I progressed through the master's degree. Furthermore, it became a great experience to learn how to design and conduct the experiment for a couple of years. Also, I would like to thank the members of the Yoo's group, both past, and present: Maulida Zakia, Merreta Noorenza Biutty, Jamin Koo, Geon Seok Lee, Farris Hilmyafif, Yubin Kim, and Seohyun Jang, for your help and support.

Pukyong National University, Busan, South Korea

February, 2022

Iseki Tissasera